Int. J. Electrochem. Sci., 9 **(2014)** 3837 - 3845

International Journal of
ELECTROCHEMICAL
SCIENCE
www.electrochemsci.org

Analysis of the Different Mechanisms of Electrochemical Energy Storage in Magnetite Nanoparticles

Álvaro León-Reyes[1], *Mauro Epifani*[2], *Teresa Chávez-Capilla*[1], *Jesús Palma*[1], *Raül Díaz*[1,*]

[1] Electrochemical Processes Unit, IMDEA Energy Institute, Avda. Ramon de la Sagra, 3, 28935 Móstoles (Madrid), Spain
[2] Istituto per la Microelettronica e i Microsistemi, IMM-CNR, Via Monteroni, 73100 Lecce, Italy
[*]E-mail: raul.diaz@imdea.org

Received: 19 November 2013 / *Accepted:* 20 March 2013 / *Published:* 14 April 2013

The use of nanostructured metal oxides as active electrode components of electrochemical energy storage devices provide benefits both from capacitive effects and from the short path lengths for faradaic processes, both of which becoming increasingly important at nanoscale dimensions. In this work, we analyze the capacitive and faradaic contributions to energy storage for Fe_3O_4 at two different nanoscale sizes in neutral aqueous media. The understanding of the contributions of each one of the effects at different sizes for different materials may provide clues for the design of devices with both high power and high energy density.

Keywords: Magnetite; energy storage; electrochemical mechanisms; composite electrodes.

1. INTRODUCTION

The massive implementation of renewable energy sources is critically depending on the development of competitive high energy density and high power density storage devices, and electrochemical technologies are the most promising to achieve this goal.

One of the main current directions to improve electrochemical energy storage devices in terms of electrode materials is the development of nanostructures, mainly because nanostructured materials offer enhanced electrochemical performance due to their ability to access both bulk and surface properties. Short path lengths for both electronic and ionic transport as well as the large active surface area, which increases both the double layer and the pseudocapacitive contributions, are believed to be the key reasons for these improvements [1]. Thus, nanostructured materials might offer the opportunity

to tailor both power density and energy density and develop an electrochemical device with the best attributes of batteries and supercapacitors.

A better understanding of the contribution of the different mechanisms to energy storage might provide clues to achieve this goal, and different nanostructured metal oxides such as MnO_2 [2], TiO_2 [3], and group V metal oxides [4] have already been the focus of research to discern the behavior of their faradaic and capacitive contributions. In this sense, nanosized Fe_3O_4, with its moderate cost, environmental friendliness, and suitable properties, is a promising alternative material in, for example, Li-ion battery anodes [5] and supercapacitors [6], but the contribution of the different mechanisms to energy storage in these oxides needs to be further explored.

Three different processes can contribute to the electrochemical performances for Fe_3O_4: (1) double-layer charging/discharging of Fe_3O_4 surfaces; (2) pseudocapacitive Faradaic processes associated with redox reactions of surface $Fe^{2+/3+}$ centers, and (3) Faradaic reactions of $Fe^{2+/3+}$ centers requiring charge compensation from electrolyte cations. In this work, we have used a detailed voltammetric analysis developed by Conway and coworkers [7] to quantify the dependence of the capacitive and faradaic processes on the size of nanocrystalline Fe_3O_4. We have applied this study to electrodes where different percentages of active material were mixed with carbon black and a binder. The results show that the methodology developed by Conway and coworkers can be extended with reasonable accuracy to composite electrodes of certain percentage ranges when correcting the contributions of the significant components of the mixture.

2. EXPERIMENTAL

2.1. Fe_3O_4 preparation

Commercial Fe_3O_4 was purchased from Sigma Aldrich (nanopowder <50 nm, >98%), while synthetic Fe_3O_4 was prepared as previously described [8], with some changes. Briefly, in a glass beaker 2.56 mmol (1.033 g) of $Fe(NO_3)_3 \cdot 9H_2O$ were dissolved in 10 mL of methanol. Then, 0.78 mL of acacH were added followed, after 15 min, by 0.35 mL of ammonia solution (30 wt% solution in water). After stirring for 24h, 2 mL of the solution were poured in 10 mL of n-dodecylamine, forming a red precipitate. The resulting slurry was heated at 100 ^oC for 1 h, and the precipitate was extracted and washed with acetone. Then it was suspended in 10 mL of oleylamine and the clear, red suspension was heated into a 45 mL autoclave for 2 h at 220 ^oC. After cooling, a black suspension was obtained. A black magnetic powder was extracted by addition of methanol and centrifugation, followed by washing with acetone and drying.

2.2. Preparation of electrodes

Slurry was prepared by mixing Fe_3O_4 and acetylene black (carbon black, acetylene, 100% compressed, >99.9%, Alfa Aesar) in a mortar by grinding with polytetrafluoroethylene (PTFE 60 wt.% dispersion in water, Sigma-Aldrich) at different weight ratios and using 2-propanol (>99.5%,

Scharlau) as dispersive medium. The resulting slurry was spread on a stainless steel mesh (AISI 3024, 97% open, Goodfellow) on 1 cm diameter disk-shaped pieces, pressed at 450 $kg.cm^{-2}$, and dried at 120ºC for 4-5 hours.

2.3. Characterization

X-ray diffraction (XRD) was carried out with a Panalytical X'Pert PRO-MPD diffractometer working with the Cu Kα radiation (λ= 1.5406Å) using a Bragg-Brentano geometry.

Transmission Electron Microscopy (TEM) observations were carried out with a Philips Tecnai 20 microscope, which works at 200 kV with a point-to-point resolution of 0.27 nm.

Porous texture was analyzed by N_2 adsorption at 77 K (Autosorb IQ2, Quantachrome Instruments). Prior to measurements, the samples were outgassed under vacuum at 120 ºC overnight. The specific surface area (S_{BET}) was calculated from the isotherm by applying the BET model.

Electrochemical measurements were performed using a Biologic VMP3 multichannel potentiostat-galvanostat (Biologic, France) coupled with EC-Lab v10.23 software using 1 M Na_2SO_4 aqueous electrolytes. Ag/AgCl was used as reference electrode and a Pt mesh was used as counterelectrode.

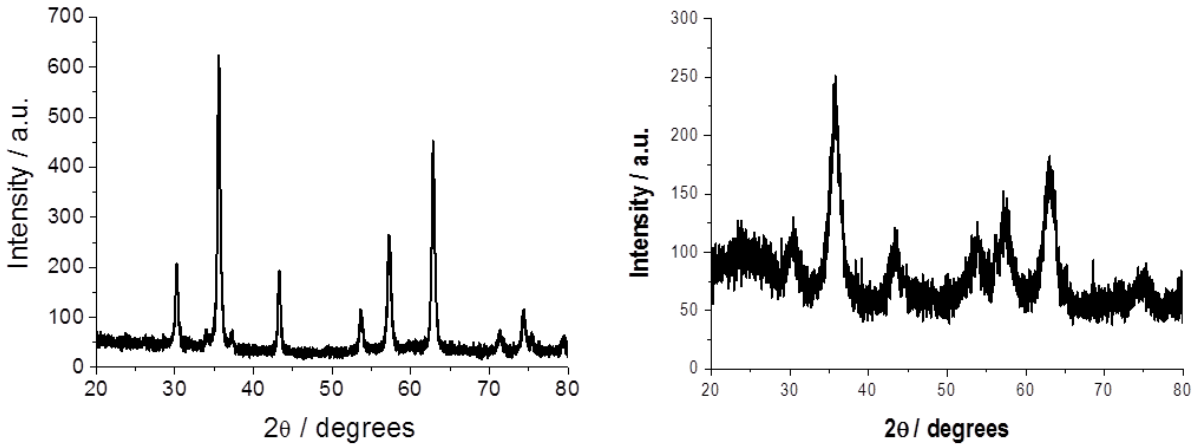

Figure 1. XRD spectra of Fe_3O_4: commercial (left) and synthetic (right).

3. RESULTS AND DISCUSSION

As the main goal of the current work is to establish the dependence of the energy storage reactions in Fe_3O_4 on the particle size, it is first important to establish the crystallinity, crystalline phase, size and surface area of the materials explored. Thus, early evaluation was carried out by X-ray diffraction (XRD). The results are shown in Fig. 1.

Both samples show the peaks of Fe_3O_4 [9], with a large broadening of the peaks in the case of the synthetic oxide which indicates the presence of small nanocrystals, whose size will be discussed in the TEM analysis below. No peaks attributable to other crystalline phases are detected.

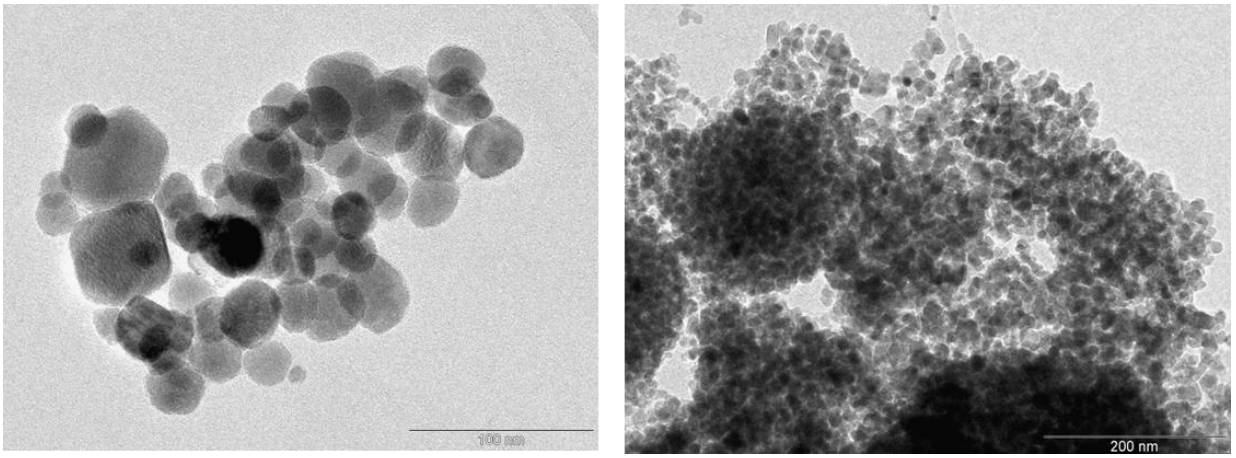

Figure 2. TEM images of Fe_3O_4: commercial (left) and synthetic (right).

The mean particle size analysis was carried out more in detail by Transmission Electron Microscopy (TEM). Representative images of the samples are shown in Fig. 2. In both cases, discrete nanoparticles with spherical shape can be clearly seen. From the analysis of the TEM images, a mean particle size of 28.6±7.5 nm for commercial Fe_3O_4 and of 13.8±3.9 nm for the synthetic one was obtained.

The specific surface areas were evaluated from nitrogen adsorption isotherms. The specific surface areas calculated using the BET approach are 40.1 m^2g^{-1} for commercial Fe_3O_4 and 59.6 m^2g^{-1} for synthetic Fe_3O_4. Thus, the surface area of the synthetic oxide is higher, in accordance with its smaller mean particle size.

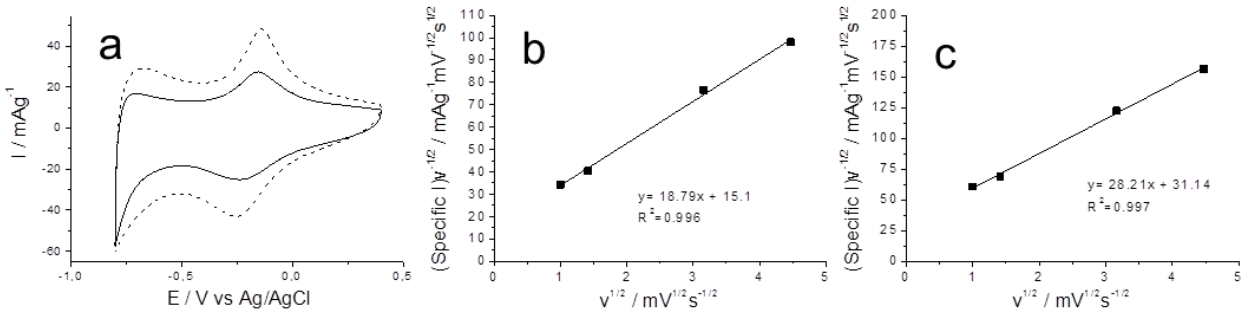

Figure 3. (a) Cyclic voltammograms at 1 mVs^{-1} of commercial (straight line) and synthetic (dashed line) Fe_3O_4; Fitting from cyclic voltammetry experiments (square symbols) at the maximum of the oxidation peak of commercial Fe_3O_4 (b) and synthetic Fe_3O_4 (c). All experiments are performed in 1 M Na_2SO_4 with electrodes where Fe_3O_4 was mixed with carbon black and PTFE in a weight ratio of 8:1:1.

The electrochemical responses were evaluated from cyclic voltammetry experiments which were performed in a three-electrode cell in 1 M Na_2SO_4 aqueous electrolyte. Both kinds of Fe_3O_4 present oxidation and reduction peaks (Fig. 3a), as previously reported in neutral aqueous electrolytes for Fe_3O_4 [10], and the bigger area under the voltammetry curves of synthetic oxide is indicative of its higher specific capacitance.

In order to study the different energy storage mechanisms at play, we performed cyclic voltammetry experiments at different scan rates for both oxides. In this way, capacitive processes can be distinguished from faradaic processes by fitting the dependence of the current (i) versus the scan rate (υ) to the following curve: $i = a\,\upsilon^{b}$, where a and b are adjustable parameters, a depending on the electrode area, concentration of $Fe^{2+/3+}$ redox centers, and diffusion coefficient for charge transport in the Fe_3O_4 [11], and b indicating the mechanism. There are two limiting values for b: when b = 0.5, the process is controlled by diffusion, while when b = 1, the processes responsible for the voltammetric response are surface-limited, including double layer charging and pseudocapacitive charge transfer at surface $Fe^{2+/3+}$ centers. Both limits can be found in voltammetries of Fe_3O_4 (Fig. 3a): at E = -0.5 V, b = 0.99, indicating that capacitive processes dominate the current, while at E ~ -0.1 V (the maximum of the oxidation peak), b = 0.5, indicating that diffusive processes dominate the current.

To have a further insight on the mechanisms at play during the whole voltammetry curve, one can follow the method developed by Conway [3] and Dunn [7] for deconvoluting the two components corresponding to the two values of b mentioned above. Thus, for a series of voltammetries performed at different scan rates, the total current measured at a certain potential i(V), is given by the sum of two components:

$$i(V) = k_1\upsilon + k_2\upsilon^{1/2} \quad (1)$$

where i is the intensity of the voltammetric curve, *v* the scan rate, and k_1 and k_2 are scan rate independent constants. As mentioned above, there are two main types of mechanism which might be present: pure capacitive processes (including double layer and pseudocapacitance) will show a linear dependence of the intensity versus the scan rate, while pure diffusion-controlled faradaic processes will show a linear dependence of the intensity versus the square root of the scan rate. Thus, in eq. 1, $k_1\upsilon$ represents the amount of capacitive processes, and $k_2\upsilon^{1/2}$ the amount of faradaic processes. Then, by determining k_1 and k_2 it is possible to quantify, at specific potentials, the fraction of the current due to each of these contributions.

Arranging equation (1) for analytical purposes one can obtain:

$$\frac{i(v)}{v^{1/2}} = k_1 v^{1/2} + k_2 \quad (2)$$

When measuring the intensity of the current at the maximum of the oxidation peak in cyclic voltammograms at different scan rates, the linear fitting in Figs. 3b and 3c can be identified with eq. 2. Thus, the linear behavior shown in these figures allows the determination of k_1 and k_2 from the slope and the y-axis intercept point respectively, thus enabling us to distinguish quantitatively between the currents arising from faradaic diffusion-limited processes and those occurring from capacitive processes. As can be clearly seen, at the oxidation peak maximum both kinds of energy storage mechanism are more important in the synthetic Fe_3O_4 and, interestingly, the ratio of k_1 (capacitive

contribution) between the commercial and the synthetic oxide coincides with the ratio of their measured surface BET areas.

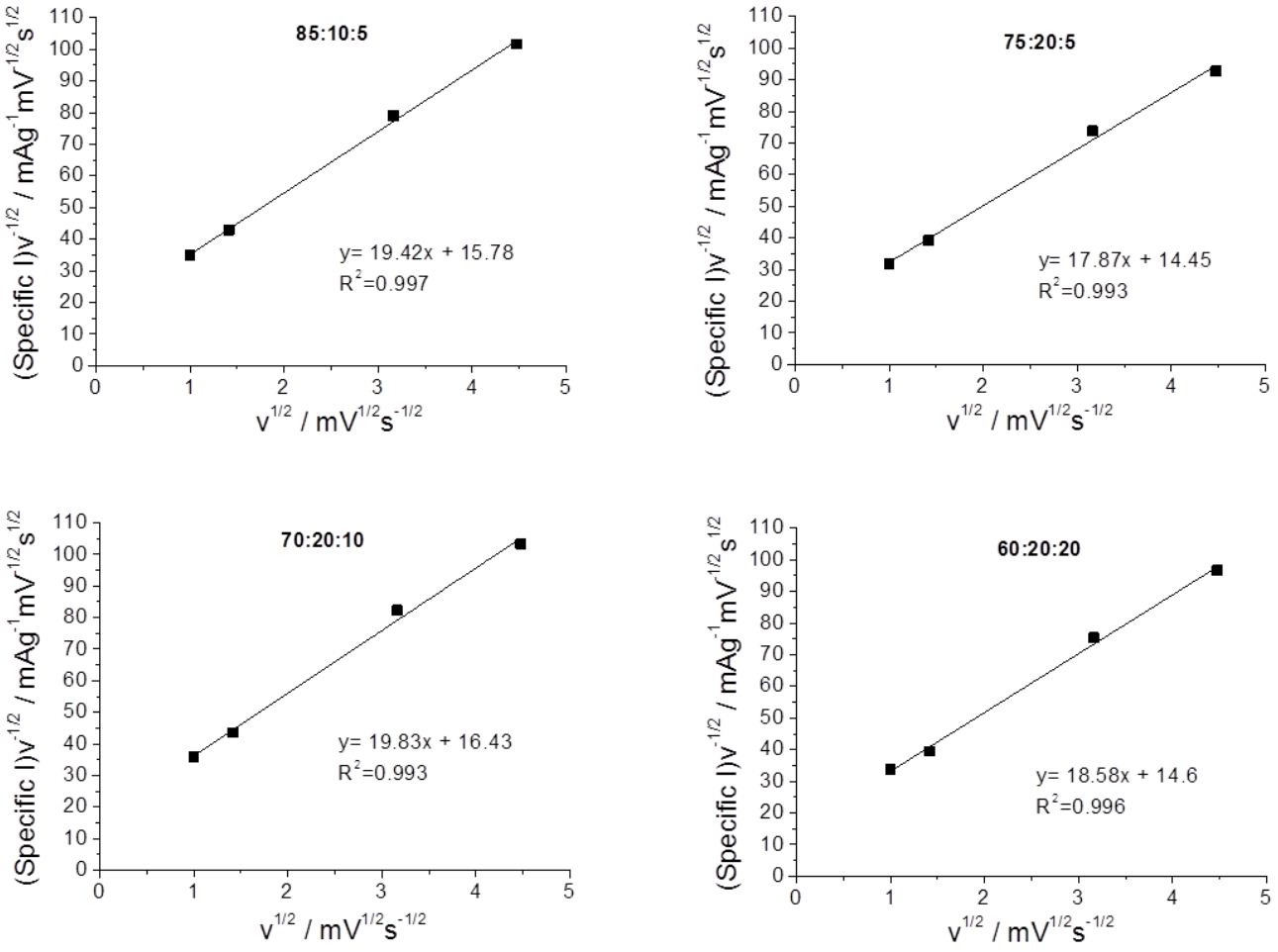

Figure 4. Fitting from cyclic voltammetry experiments (square symbols) at the maximum of the oxidation peak of commercial Fe_3O_4. All experiments are performed in 1 M Na_2SO_4 with electrodes where Fe_3O_4 was mixed with carbon black and PTFE in different weight percentages specified in each figure as Fe_3O_4:CB:PTFE.

While the method to discern between different reaction mechanisms in a certain material was developed by Conway and coworkers using a pure material [7] and until now has been applied only to pure materials [2-4], our results are calculated from the voltammetries of Fe_3O_4 electrodes mixed with carbon black as conducting additive and PTFE as a binder in a weight ratio of 8:1:1. The specific intensities of Figs. 3b and 3c are normalized to the weight of Fe_3O_4, and the intensity value used for the figures and the fittings has been calculated after subtracting the weighted intensity value of the cyclic voltammetries of pure carbon black in the same experimental conditions. We performed further experiments with commercial Fe_3O_4 electrodes prepared with mixtures of different weight percentages ranging from 5 to 20% of carbon black and PTFE. The fitting results after subtracting the weighted contribution of carbon black provide the same significant parameters within the experimental error (see fig. 4).

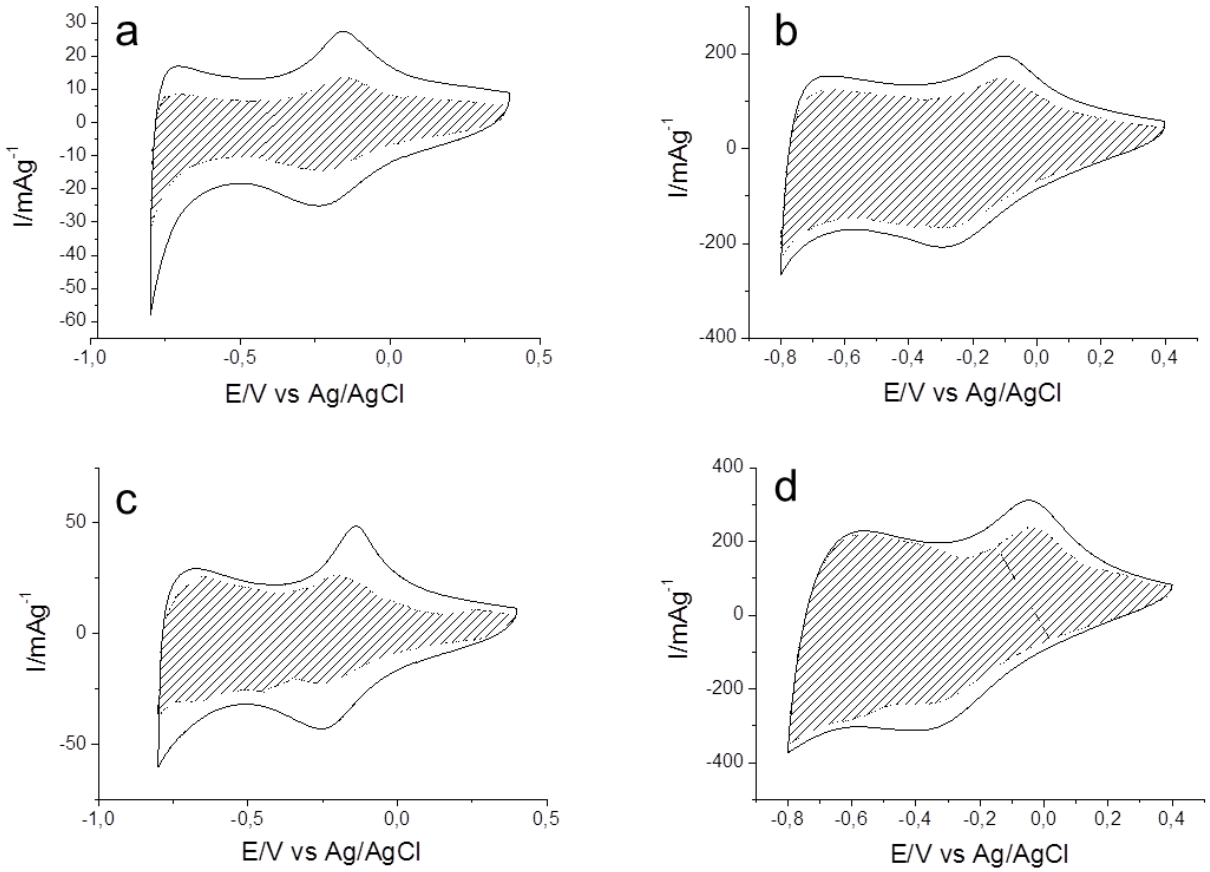

Figure 5. Cyclic voltammograms of commercial Fe_3O_4 at: (a) 1 mVs^{-1} and (b) 10 mVs^{-1}, and of synthetic Fe_3O_4 at: (c) 1 mVs^{-1} and (d) 10 mVs^{-1}. In all of them, the dashed areas represent the capacitive contribution to the total stored energy.

To obtain a further insight on the storage mechanisms present in Fe_3O_4, we further deconvolute both kind of storage mechanism during the whole cyclic voltammetry and at two different scan rates. Thus, Fig. 5 shows the voltage profile for the (pseudo)capacitive currents (dashed area) compared with the total measured currents as obtained from the voltammetric response for the two Fe_3O_4 and at two different scan rates. At low scan rates (Figs. 5a and 5c) it is evident that far greater capacitive currents are observed for the synthetic Fe_3O_4 due to its smaller particle size. These results are consistent with those in Fig. 3b and 3c in that the diffusion-controlled faradaic processes are dominant at the peak potentials (b ~ 0.5), but capacitive currents are the main contribution at potentials away from peaks (b ~ 0.8-1).

From the data in Fig. 5 it is possible to determine the total stored charge and the relative contributions associated with diffusion controlled and capacitive processes. Thus, Figs. 5a and 5c show that, at 1 mVs^{-1}, the total energy stored is 32 Fg^{-1} for the commercial Fe_3O_4 and 51 Fg^{-1} for the synthetic one. In addition, the capacitive effects contribution from the smaller particles to the total storage is significantly higher than that from the larger particles.

The scan rate dependence of this deconvolution is of particular interest (Fig. 5b and 5d). In this case, at 10 mVs^{-1}, the total energy stored is 25 Fg^{-1} for the commercial Fe_3O_4 and 36 Fg^{-1} for the synthetic one. Thus,, while the capacitive contribution is virtually scan-rate independent for both particle sizes, the diffusion-controlled one and the total stored charge decrease with increasing scan rate.

4. CONCLUSIONS

In the current work it has been shown that at smaller nanoparticle sizes the capacitive contribution to charge storage in Fe_3O_4, including double layer and pseudocapacitive, increase, while it is virtually scan-rate independent for a wide range of particle sizes and scan rates. On the other hand, the total energy stored and the diffusion-controlled contribution are dependent on the scan rate and the particle size, increasing at lower scan rates and in synthetic Fe_3O_4 due to its smaller particle size. This analysis has been shown to be valid for composite electrodes when appropriate precautions are taken, and can be extended to other materials and become a valuable tool for the understanding and optimization of supercapacitors and other electrochemical energy storage devices based on similar materials.

ACKNOWLEDGEMENTS

The research leading to these results has received funding from the European's Community Framework Programme FP7/2007-2013 under grant agreement No. 241405. The authors also acknowledge MINECO ENE2011-22556, and SOLAR project DM19447, and R. D. acknowledges financial support from the MINECO in the Ramón y Cajal Program. Fernando Picó and María Eugenia di Falco, at IMDEA Energy Institute, are also acknowledged for their help with some characterization measurements.

References

1. A. S. Arico, P. Bruce, B. Scrosati, J. M. Tarascon and W. van Schalwijk, *Nat. Mater.* 4 (2005) 366.
2. W. Yan, T. Ayvazian, J. Kim, Y. Liu, K. C. Donavan, W. Xing, Y. Yang, J. C. Hemminger and R. M. Penner, *ACS Nano* 5 (2011) 8275.
3. J. Wang, J. Polleux, J. Lim and B. Dunn, *J. Phys. Chem. B* 111 (2007) 14925.
4. K. Brezesinski, J. Wang, J. Haetge, C. Reitz, S. O. Steinmueller, S. H. Tolbert, B. M. Smarsly, B. Dunn and T. Brezesinski, *J. Amer. Chem. Soc.* 132 (2010) 6982.
5. (a) P. Poizot, S. Laruelle, S. Grugeon, L. Dupont and J. M. Tarascon, *Nature* 407 (2000) 496; (b) P. L. Taberna, S. Mitra, P. Poizot, P. Simon and J. M. Tarascon, *Nat. Mater.* 5 (2006) 567.
6. M. B. Sassin, A. N. Mansour, K. A. Pettigrew, D. R. Rolison and J. W. Long, *ACS Nano* 4 (2010) 4505.
7. T. C. Liu, W. G. Pell, B. E. Conway and S. L. Roberson, *J. Electrochem. Soc.* 145 (1998) 1882.
8. M. Epifani, J. Arbiol, T. Andreu and J. R. Morante, *Cryst. Growth Des.* 10 (2010) 5176.
9. JCPDS file no. 19-0629.

10. (a) T. Cottineau, M. Toupin, T. Delahaye, T. Brousse and D. Bélanger, *Appl. Phys. A: Mater. Sci. Process*. 82 (2006) 599; (b) S. Y. Wang, K. C. Ho, S. L. Kuo, N. L. Wu, *J. Electrochem. Soc.* 153 (2006) A75.
11. A. J. Bard and L. R. Faulkner, *Electrochemical Methods: Fundamentals and Applications*, 2nd ed., Wiley, New York (2001).